Design and Implementation of a Low Cost Isotropic Electric Field Sensor for SAR Measurements

Marco Quispe ⓘD , Javier Samaniego ⓘD , Jorge Olivares ⓘD , Rolando Adriano ⓘD , B. Pérez ⓘD , and Saúl Inca ⓘD

Abstract—Specific Absorption Rate (SAR) measurement systems are used to evaluate exposure to fields radiated by wireless devices placed close to people's bodies. One of the fundamental elements of these systems is an isotropic electric field sensor that is small relative to the radiated wavelength. The obtained SAR value must be compared with the basic restriction levels or exposure limits established by the International Commission on Non-Ionizing Radiation Protection (ICNIRP) or similar international bodies. This work presents the design and implementation of a novel isotropic electric field sensor made with low-cost materials and processes. The response of the developed sensor was compared with the response of a commercial probe in order to perform calibration. The calibration methodology proposed in this work allows transforming voltage measured with the developed low-cost probe to electric field values measured with a calibrated commercial probe in order to calculate SAR values. The results show that the developed sensor can be used in SAR measurement processes.

Link to graphical and video abstracts, and to code: https://latamt.ieeer9.org/index.php/transactions/article/view/9088

Index Terms—SAR Probe, Electric Field Measurements, Detector Diode, ICNIRP.

I. INTRODUCTION

Exposure to non-ionizing radiation sources generated by wireless communications devices causes an increase in people's body temperature [1]. Current scientific evidence indicates that this increase will not have adverse effects on people's health if the exposure level is below the limit values established by the ICNIRP [2]. To quantify the absorption of the body's tissues to the emissions generated by communication equipment at frequencies below 6 GHz, the SAR parameter is used, while for higher frequencies the Absorbed Power Density (APD) magnitude is considered [1]. Wireless communication equipment that is placed on or near the body generates radiation that interacts with the body's tissues, generating a thermal effect. This exposure must be evaluated before a product is marketed to ensure that people are not exposed, during its use, to radiation levels higher than

M. Quispe, J. Samaniego, J. Olivares, and B. Pérez are with Universidad Nacional de Ingeniería, Lima, Perú (e-mails: mquispe@inictel-uni.edu.pe, jsamaniego@inictel-uni.edu.pe, jolivares@inictel-uni.edu.pe, and bperez@uni.edu.pe).

R. Adriano is with Universidad Nacional Mayor de San Marcos, Lima, Perú (e-mail:'radrianop@unmsm.edu.pe)

S. Inca is with Universidad Politécnica de Valencia, Valencia, Spain (e-mail:sauin@iteam.upv.es).

those established in the ICNIRP recommendations. For this purpose, if applicable, the SAR measurement is carried out in certified and independent laboratories. These laboratories have specialized and expensive equipment that allows precise and repetitive measurements. Within this set of equipment there is a SAR probe whose tip is positioned in different locations within a volume filled with a liquid during measurements. These probes must be calibrated at the frequency at which they will be evaluated, considering the liquid in which the measurements will be made and taking into account correction factors determined by the communication technology implemented by the evaluated equipment. Because these systems are expensive, some works have proposed the development of low-cost measurement systems. An example of this can be seen in [3], where a SAR measurement system is developed except for the probe and a simulation. In the same sense, in [4], an alternative simulation approach to evaluate SAR is presented. This work presents the design and development of a low-cost electric field sensor that can be used in SAR measurement systems in some of the main frequency bands used in mobile communications (900 MHz, 1800 MHz and 3500 MHz). Likewise, a calibration procedure is proposed that must be carried out to convert the electrical voltage values acquired with the implemented sensor, which is called IU sensor, to reliable electric field values obtained with a commercial probe, called MVG probe.

II. SAR MEASUREMENT SYSTEMS

SAR measurements are performed using a robotic arm that carries an electric field measurement probe whose tip is located at different positions within a volume containing a liquid that has dielectric properties (permittivity and conductivity) similar to head tissues. The volume of liquid is contained within a shell of dielectric material, called phantom, that has a shape similar to a human head (SAM - Specific Anthropomorphic Mannequin) [5] as shown in Fig. 1. Measurements are controlled by software that runs on a computer.

The electrical voltage values at the output of the probe are measured by a high sensitivity bench multimeter controlled by the computer which calculates the SAR and presents the results. The measurement system is located inside a Faraday cage for electromagnetic isolation from external radio frequencies.

A SAR measurement probe consists of three electrically short dipole antennas arranged in space in such a way that together they present isotropic behavior. A Schottky diode is placed in the center of each antenna. At the ends of the diode,
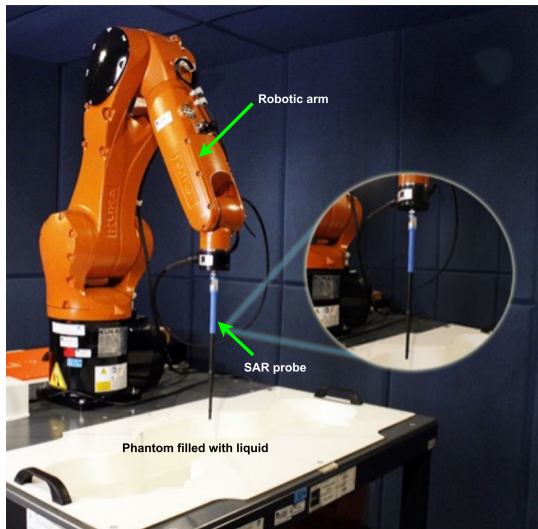
Fig. 1. SAR measurement system.

a pair of high-impedance non-metallic conductive transmission lines are originated. High frequency Schottky diodes are used to take advantage of their quadratic response region. In [6], for example, the HSMS2850 diode is used as a radio frequency detector.

All these elements are placed on each of the faces of a triangular section prism made of ceramic material. At the other end of the transmission lines, an acquisition system or a high sensitivity multimeter is connected. The probe is placed inside a container made of material transparent to electromagnetic waves, with a dielectric constant at least 5 times lower than the dielectric constant of the liquid medium in which it will be inserted. In [5] the technical characteristics that must be met by probes for SAR measurement at different frequencies are mentioned. Short dipoles are used to achieve adequate spatial resolution during measurements, reducing the edge effect and not altering significantly the distribution of the existing electric field. This is highlighted in [7] and [8] where the development of a sensor that allows electric field measurements up to 20 GHz is presented.

When RF energy impinges the probe, a voltage is induced and the measurement is carried out. The voltage is conducted through high impedance resistive lines to a highly sensitive multimeter (microvolt scale). These measurements are sent to a computer that estimates SAR based on the measured voltage values, calibration factors of the probe, and the conductivity and mass density of the liquid used to simulate a tissue at a frequency of interest. Calibration factors allow electric field values to be obtained from voltage values measured by the probe when it is inside the liquid. Procedures for finding probe calibration factors are described in [9], [10] and [11].

III. DESIGN AND IMPLEMENTATION OF ISOTROPIC ELECTRIC FIELD SENSOR

A. SAR Measurement System at INICTEL-UNI

The INICTEL-UNI is a national institute for research and training in telecommunications in Perú. It has an SAR measurement system model COMOSAR v5 from the manufacturer
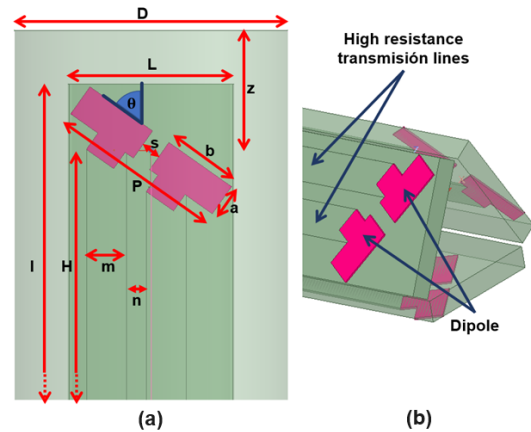

Fig. 2. Views of the geometry of the developed electric field sensor.

MVG (Microwave Vision Group) which consist of an electric field measurement probe with an operating range of 30 MHz to 3000 MHz, a KUKA robotic arm and its control system, a Keithley model 2000 multimeter, a computer with OpenSAR software and the necessary communication interfaces to carry out the measurement in an automated way. Likewise, it has reference dipole antennas of 900 MHz, 1800 MHz, 3500 MHz and liquids that simulate the tissue of the human head at these frequencies [12].

B. SAR Probe Design

The sensor is composed of three short dipole antennas arranged in space as shown in Fig. 2. A small, high-frequency Schottky diode was placed in the middle of the antennas. The ends of the diodes were connected to a highly sensitive measurement system through non-metallic conductive lines implemented with carbon ink. These elements were placed on a 0.4 mm thick fiberglass plate used to make printed circuits. The dimensions of the sensor tip are presented in Fig. 2 and Table 1. The outer diameter of the tip of the sensor housing is denoted by the letter *D*. The sensor offset is the distance between the center of the dipole antenna and the outer surface of the probe base, *z*. The length of the dipole, *P*, is the sum of the lengths of the dipole arms and the separation space between them. The geometry and dimensions of the sensor were determined taking [5] as reference.

C. Effect of using the Sensor on the Electric Field Distribution within a Phantom

In order to evaluate the influence of the presence of the sensor on the existing electric field, the scenario shown in Fig. 3 was simulated using the 3D electromagnetic phenomenon simulation software called Ansys HFSS [13]. The scenario consists of a 1800 MHz reference dipole antenna radiating a power of 17 dBm and placed in front of a hemispherical phantom filled with a liquid with a relative vacuum permittivity of 40 and a conductivity of 1.4 S/m. The virtual phantom had a diameter of 20 cm, a depth of 10 cm and a shell with a thickness of 2mm with a relative permittivity of 1.1. The shell material has been chosen so that it is transparent to radiofrequency waves while its diameter is comparable to that

TABLE I
SAR PROBE DIMENSIONS

| Parameter	Symbol	Value
Antenna width	a	0.5mm
Separation width between dipole arms	s	0.6mm
Total dipole length	P	2.7mm
Dipole inclination angle with respect to vertical	θ	54.74°
Copper thickness on PCB board	e	0.035mm
PCB board thickness	e	0.4mm
PCB board length	E	165mm
PCB board width	L	2.7 mm
PCB material	-	Fiberglass
Transmission line material	-	Carbon ink
Transmission line length	H	155 mm
Separation between transmission lines	n	1.27 mm
Probe cover material	-	Polylactic Acid (PLA)
Probe tip diameter	D	6 mm
Probe cover thickness	c	1 mm
Distance from dipole center to outer surface of probe base	z	2.3 mm
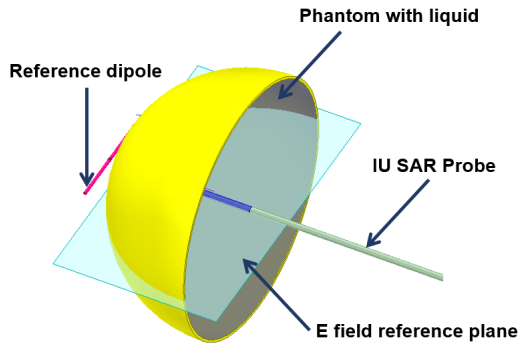
Fig. 3. Simulated scenario.

of an adult's head. Through simulation, the distribution of the electric field in a plane containing the reference dipole antenna (E field reference plane) and the designed sensor was determined, considering a scenario with the sensor and another without a sensor, are shown in part (b) and (a) of Fig. 4 respectively. For both cases it is observed that the maximum values of the magnitude of the electric field inside the phantom are between 56 V/m and 70 V/m. Because this difference (about 2 dB) is small for signals that propagate in air, it can be stated that the insertion of the sensor into the scenario does not significantly alter the distribution or magnitude of the electric field in the phantom.

D. Electric Field Sensor Implementation

The PCB layout of a short dipole antenna of 2.7mm length was prepared for its implementation on a 0.4 mm fiberglass printed circuit strip of thickness using the Eagle software. The dimensions of the strip were 16.5 cm long and 2.7 mm wide. An SMD Schottky diode was soldered in the center of the antenna. From the ends of the diode, a pair of non-metallic conductive lines, implemented with carbon ink and impregnated to the fiberglass by a process of screen printing and curing with ultraviolet light, were drawn. This is in order to obtain quick drying and more robust lines as shown in part b of the Fig. 5. Three replicas of this set were made and placed on each of the faces of a prism with a triangular section implemented with 3D printing using Polylactic Acid
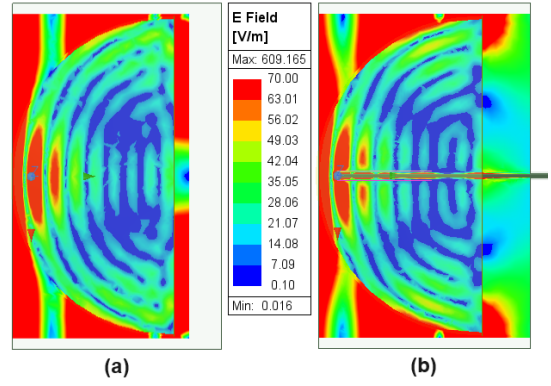

Fig. 4. Electric field distribution in phantom in absence (a) and presence of SAR probe (b).
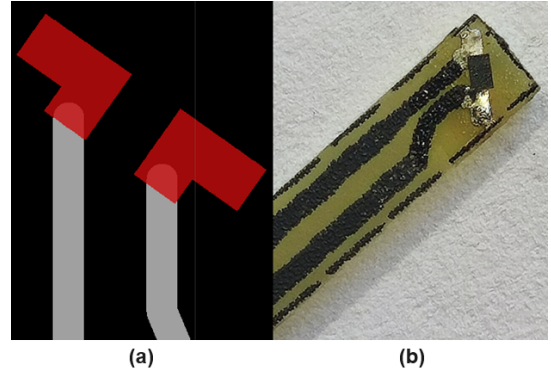

Fig. 5. Detailed view of one of the dipoles at the tip of the probe. Eagle layout (a), deployed probe (b).

(PLA) material. This set was placed in a container, also 3D printed, made of PLA. In order to facilitate the construction process, the dipole antennas were first implemented and screen printed with carbon ink on a printed circuit board 20 cm long and 20 cm wide. Then, the PCB was cut to obtain the small strips indicated above. The carbon ink used was SD 2842 HAL from the manufacturer PETERS, which has a resistance that will depend on the curing method used. In the present work, the Schottky diode BAT1502ELE6327XTMA1 from Infineon Technologies was used because it has physical dimensions suitable for the development of power sensors in near field. Because the implemented sensor had to be integrated into the existing SAR measurement system at INICTEL-UNI, this sensor also had to have physical compatibility with the connector of that system. The SR30-10PG-6P(31) connector from manufacturer Hirose Electric Co Ltd was identified as meeting this requirement.

IV. VERIFICATION OF THE IMPLEMENTED ELECTRIC FIELD SENSOR

A. Test Setup

The SAR measurement system was used to compare the response of the developed sensor, called IU, with the response of the existing SAR system probe, called MVG. The frequencies considered for this comparison were 900 MHz, 1800 MHz and 3500 MHz.

The Fig. 6 shows the implemented test setup. There, a generator connected, through an RF cable, to a reference
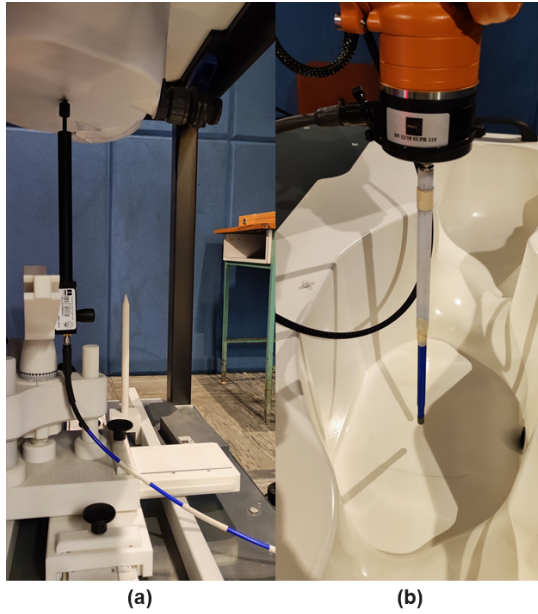
(a)   **(b)**

Fig. 6. Scenario implemented for evaluation of the SAR probe. Reference dipole antenna (a) and IU sensor on robotic arm (b).
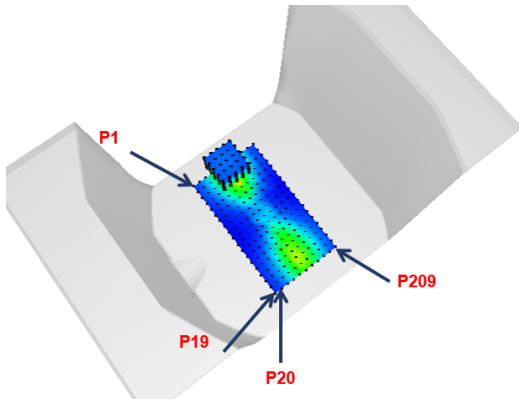

Fig. 7. Mesh of measuring points.

dipole antenna which radiated an unmodulated carrier signal at one of the three frequencies of interest. The output power of the generator was set at 16 dBm. A reference dipole antenna corresponding to the evaluated frequency was placed just below the flat part of the phantom. The IU sensor and the MVG probe were placed alternately on the robotic arm of the SAR system. Then, the OpenSAR software of the SAR system was run and the voltage measurements at the output of each of the axis of the evaluated probe were recorded. During the measurements the phantom was empty, without liquid.

The OpenSAR software establishes that, as the first phase of the SAR measurement process, measurements must be made on a mesh of points located on a plane parallel to the base of the flat part of the phantom, 4mm above the base. The mesh has 209 points in total (11 elements on the X axis and 19 elements on the Y axis). The mesh resolution is 8 mm in the x and y axes. This mesh and the order in which measurements are made at the points that make up the mesh (P1 to P209) are presented in Fig. 7.
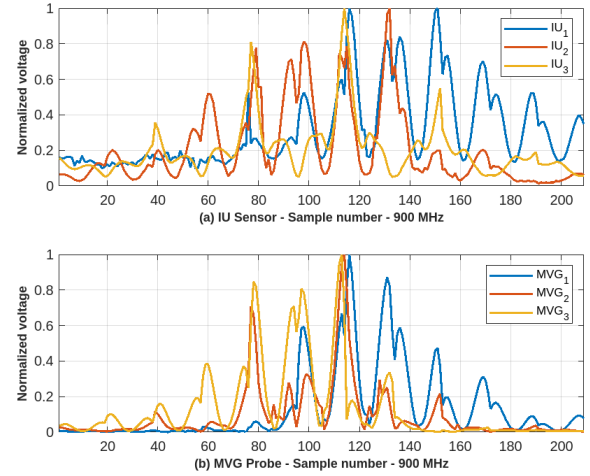

Fig. 8. (a) Normalized voltages of the three short dipole antennas of the IU sensor and (b) MVG probe at 900 MHz.
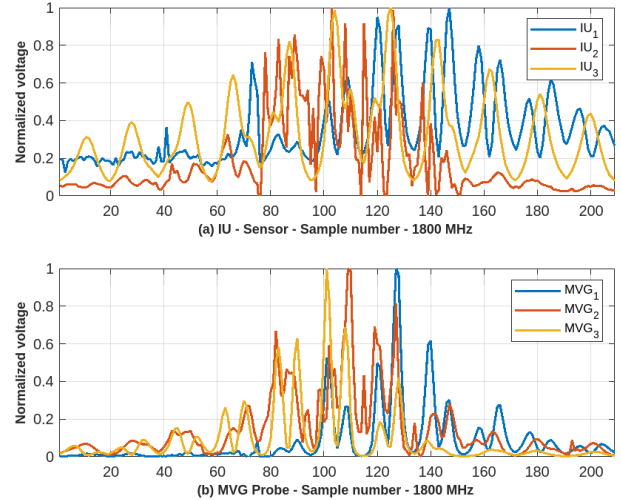

Fig. 9. (a) Normalized voltages of the three short dipole antennas of the IU sensor and (b) MVG probe at 1800 MHz.

B. Results

Part (a) of Fig. 8, Fig. 9 and Fig. 10 display the normalized voltages at the output of each of the IU sensor antennas (IU1, IU2 and IU3) and the part (b) display the normalized voltages at the output of the MVG probe antennas (MVG1, MVG2 and MVG3), for the frequencies of 900 MHz, 1800 MHz and 3500 MHz respectively.

It is observed that the curves corresponding to the IU sensor and the MVG probe present similar trends but differ in their numerical values. Likewise, for antenna IU1, the relative difference between the maximum measured value and the minimum value is lower with respect to antennas IU2 and IU3. This is because the development of each of the antennas was carried out using non-automated processes. This is true for all three frequencies evaluated. It is necessary to apply a calibration process to convert the values measured with the IU sensor to true values obtained with the MVG probe.

V. CALCULATION OF CALIBRATION FACTORS

In general, the voltage between the terminals of the Schottky diodes, v_i, of the probe and the measured electric field, E_i, are related by Eq. (1) [14].
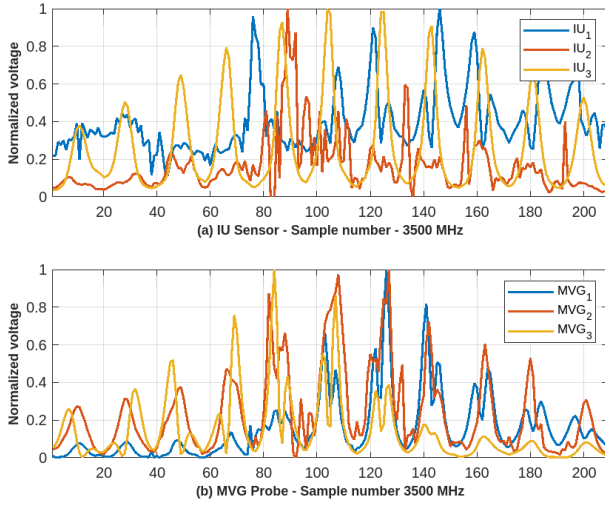
Fig. 10. (a) Normalized voltages of the three short dipole antennas of the IU sensor and (b) MVG probe at 3500 MHz.

$$E = \sqrt{\sum_{i=1}^{3} \frac{v_i}{k_i}} = \sqrt{\sum_{i=1}^{3} E_i^2} \qquad (1)$$

Where the k_i values are the antenna calibration factors, whose value depends on the evaluated frequency and the composition of the probe. According to Eq. (1), the square root of the weighted sum of the voltages is equal to the magnitude of the evaluated electric field.

It is desired to adjust the values measured by the IU sensor to reliable values measured with the MVG probe, so Eq. (2) is defined.

$$\sum_{i=1}^{3} \frac{v_{i\_IU}}{k_{i\_IU}} = \sum_{i=1}^{3} \frac{v_{i\_MVG}}{k_{i\_MVG}} \qquad (2)$$

The constants k_{i_MVG} are specific to the MVG probe and are provided by the manufacturer while the values of k_{i_IU}, corresponding to the IU sensor, must be found.

The MVG sensor used has the following values: $k_{1\_MVG} = 5.28 \ \mu \ V/(V/m)^2$, $k_{2\_MVG} = 6.28 \ \mu \ V/(V/m)^2$ and $k_{3\_MVG} = 6.54 \ \mu \ V/(V/m)^2$.

On the other hand, v_{i_IU} and v_{i_MVG} represent the voltages at the output of each of the three elements of the developed IU sensor and the MVG probe, respectively.

Measurements were made at the 209 points of the mesh showed in the Fig. 7 in order to find the most appropriate values of k_{i_IU} through a comparison process explained below. This number of points or samples is the maximum that the SAR system used allows measurement when carrying out evaluations on a surface. For each of the 209 measured points, the variable K_n is defined according to Eq. (3)

$$K_n = \sum_{i=1}^{3} \frac{v_{i,n\_MVG}}{k_{i\_MVG}} = \sum_{i=1}^{3} \frac{v_{i,n\_IU}}{k_{i\_IU}} \qquad (3)$$

$n = 1, 2, \ldots, 209$

The objective was to find the best values of k_{i_IU} that best satisfy Eq. (3) for the 209 points measured. To do this, the measurements made are arranged in a matrix as expressed in Eq. (4). The objective is to have a linear system of equations
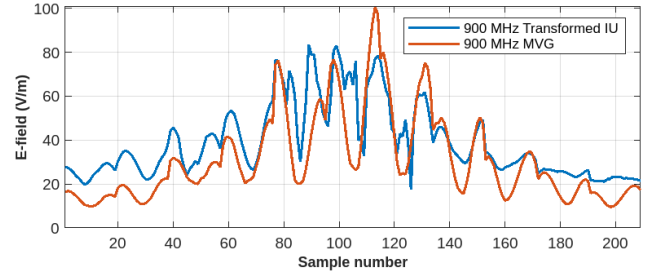

Fig. 11. MVG vs IU electric field values at 900 MHz.

in which the variables are m, n and p. Where: $m = \frac{1}{k_{1\_IU}}$, $n = \frac{1}{k_{2\_IU}}$ and $p = \frac{1}{k_{3\_IU}}$

$$\begin{pmatrix} v_{1,1\_IU} & v_{2,1\_IU} & v_{3,1\_IU} \\ v_{1,2\_IU} & v_{2,2\_IU} & v_{3,2\_IU} \\ \vdots & \vdots & \vdots \\ v_{1,209\_IU} & v_{2,209\_IU} & v_{3,209\_IU} \end{pmatrix} \begin{pmatrix} m \\ n \\ p \end{pmatrix} = \begin{pmatrix} K_1 \\ K_2 \\ \vdots \\ K_{209} \end{pmatrix} \qquad (4)$$

After the measurements were carried out, they were ordered according to Eq. (4) to find the solution of the system, that is, the values of k_{1_IU}, k_{2_IU} and k_{3_IU}. The values found are presented in Table 2.

TABLE II
VALUES FOUND OF k_{1_IU}, k_{2_IU} AND k_{3_IU}. IN $uV/(V/m)^2$

Frequency (MHz)	k_{1_IU}	k_{2_IU}	k_{3_IU}
900	-68.14	0.89	1.15
1800	1.89	2.94	10.73
3500	7.76	2.07	0.77

VI. VALIDATION OF RESULTS

In order to verify the validity of the calibration factors found, 209 measurements were carried out again with the IU sensor and the MVG probe. The calibration factors found were applied to the values measured with the IU sensor and compared with the new values measured with the MVG probe (true values). This comparison is shown graphically in Fig. 11, Fig. 12 and Fig. 13. Similar trends are observed in the curves corresponding to the values of the MVG probe and the IU sensor with their transformed values. This is despite the fact that the IU1, IU2 and IU3 antennas did not have exactly the same construction. The difference between the values measured by the MVG probe and the developed sensor differs to a greater magnitude in some sections of the curves presented because the location in space of the three antennas contained in the MVG probe was not known and therefore did not coincide. necessarily with the location of the antennas IU1, IU2 and IU3 of the developed sensor when these were used with the SAR measurement system. This determines that the developed sensor can be used in electric field measurements in the near field of an antenna.

The CDF (Cumulative Distribution Function) of the absolute error is shown in Fig. 14, in V/m. The error is calculated as the difference between the electric field values calculated using the measured voltages with the MVG and the the estimated electric field values using the voltages obtained from the measurements made with the developed IU sensor for 900 MHz, 1800 MHz and 3500 MHz. The 50th percentile for the curves presented
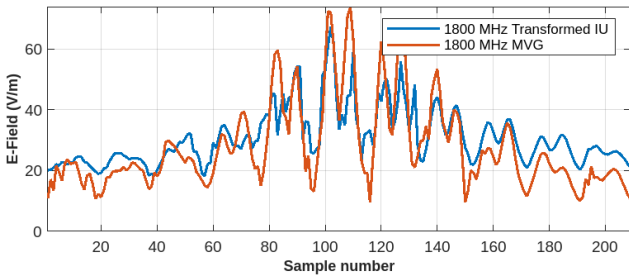
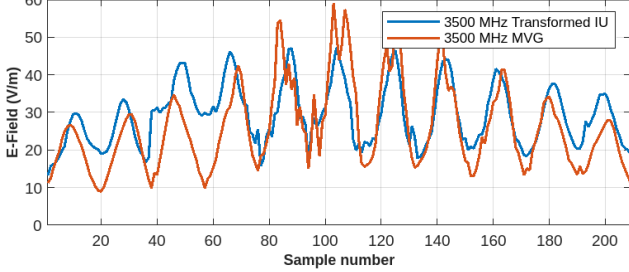Fig. 12. MVG vs IU electric field values at 1800 MHz.

Fig. 13. MVG vs IU electric field values at 3500 MHz.

Fig. 14. CDF of absolute error for 900 MHz, 1800 MHz and 3500 MHz.

indicates that 50% of the estimates for 3500 MHz and 1800 MHz have an error less than 5.7 V/m. In the case of 900 MHz, 50% of the samples have an error of less than approximately 9.6 V/m. For the 900 MHz frequency, it is observed that 90% of the estimated values have an error less than or equal to 17.5 V/m. For 1800 MHz, 90% of the estimated values have an error less than or equal to 14.27 V/m while in the case of 3500 MHz, 90% of the values estimated with the IU sensor have an error less than or equal to 12.45 V/m. A decrease in the error is observed as the frequency increases.

A. Effect of Error in Calculated Electric Field over SAR Values

The SAR value is given by Eq. (5) [15]. There, E is the rms value of electric field strength, σ is the electrical conductivity and ρ is the mass density of the tissue.

$$SAR = \frac{\sigma |E|^2}{\rho} \tag{5}$$

The errors in terms of SAR are given by the difference of the squares of real and estimated field strengths, multiplied by the conductivity and divided by the mass density of a tissue, as expressed in Eq. (6) and Eq. (7).

$$SAR_{err} = SAR_{MVG} - SAR_{IU} \tag{6}$$

$$SAR_{err} = \frac{\sigma |E_{MVG}|^2}{\rho} - \frac{\sigma |E_{IU}|^2}{\rho} \tag{7}$$

Data of brain tissue is used to calculate SAR values. According to [16], the brain conductivity and mass density is 0.765 S/m and 1038 Kg/m^3 respectively, for example. In Eq. (7), it can be seen that the magnitude of the error in the SAR measurement depends on the difference of the squares of the field strengths obtained with the MVG probe and the IU sensor. Also, according to Eq. (1), this is equal to the difference between the sums of the voltages measured by the MVG probe and the IU sensor, weighted by the calibration factors. This determines that the error in the SAR measurement
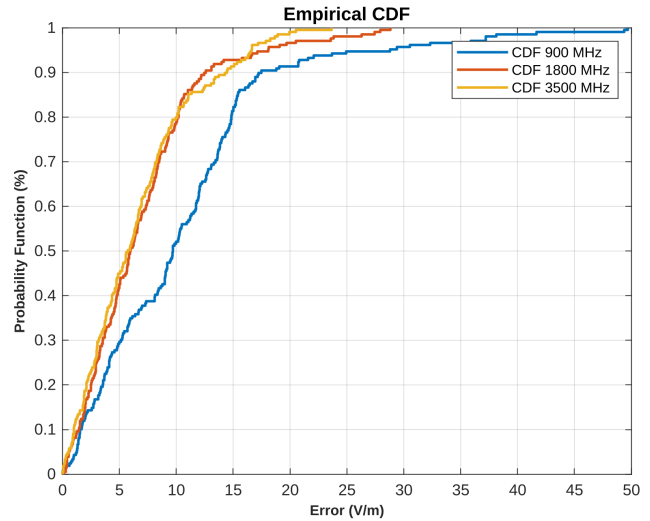
is directly proportional to the magnitude of the error of the voltages measured by the MVG probe and the IU sensor.

VII. CONCLUSIONS

The cost of the devices and materials as well as the processes carried out to implement the sensor and its housing is very low in relation to commercial products.

A procedure is presented to transform values of voltage measured with the developed low-cost experimental sensor to electric field values close to the real ones, measured with a reference SAR probe.

The minimum values of electric field intensity measured with the MVG probe are lower than the minimum values measured with the developed sensor. This determines that the MVG probe allows measuring lower values of electric field intensity.

The voltage values obtained after the transformation of the measured values with the developed sensor can then be used by the SAR system software to find SAR values.

The implemented isotropic probe presents a response to electric field variations so, once calibrated, it can be used to perform SAR measurements.

REFERENCES

[1] ICNIRP, "Guidelines for limiting exposure to electromagnetic fields (100 KHz to 300 GHz)," *Health Physics*, vol. 118, no. 5, pp. 483–524, 2020. https://doi.org/10.1097/hp.0000000000001210.

[2] R. Ramirez-Vazquez, I. Escobar, G. A. Vandenbosch, and E. Arribas, "Personal exposure to radiofrequency electromagnetic fields: A comparative analysis of international, national, and regional guidelines," *Environmental Research*, vol. 246, p. 118124, 2024. https://doi.org/10.1016/j.envres.2024.118124.

[3] S. Rodriguez, A. Gallego, E. Pineda Vargas, J. González, M. Pérez Cerquera, F. Roman, and J. Quijano, "Low-cost setup for electromagnetic SAR evaluation in a human phantom," 05 2022. https://doi.org/10.23919/EuCAP53622.2022.9769318.

[4] D. Rano, A. Yelizarov, A. Skuridin, and E. Zakirova, "Cost-effective approach for the determination of specific absorption rate of liquid phantom," in *2021 15th European Conference on Antennas and Propagation (EuCAP)*, pp. 1–5, 2021. https://doi.org/10.23919/EuCAP51087.2021.9410933.

[5] IEC/IEEE, "IEC/IEEE International Standard - Measurement procedure for the assessment of specific absorption rate of human exposure to radio frequency fields from hand-held and body-mounted wireless communication devices – part 1528: Human models, instrumentation, and procedures (frequency range of 4 MHz to 10 GHz)," *IEC/IEEE 62209-1528:2020*, pp. 1–284, 2020. https://doi.org/10.1109/IEEESTD.2020.9231298.

[6] X. Fan, X. Pei, and X. Xiong, "Zero bias Schottky diodes use in high performance detection circuits," in *Proceedings of 2011 International Conference on Electronics and Optoelectronics*, vol. 3, pp. V3–27–V3–30, 2011. https://doi.org/10.1109/ICEOE.2011.6013291.

[7] J. Wojcik and P. Cardinal, "New advanced methodology for near field measurements for SAR and antenna development," in *1999 IEEE International Symposium on Electromagnetic Compatability. Symposium Record (Cat. No.99CH36261)*, vol. 2, pp. 909–913 vol.2, 1999. https://doi.org/10.1109/ISEMC.1999.810178.

[8] K. Pokovic, T. Schmid, and N. Kuster, "Millimeter-resolution E-field probe for isotropic measurement in lossy media between 100 MHz and 20 GHz," *IEEE Transactions on Instrumentation and Measurement*, vol. 49, no. 4, pp. 873–878, 2000. https://doi.org/10.1109/19.863941.

[9] D. Qi, Z. Yu, J. Zhao, and F. Zou, "A calibration of E-field probe based on tissue-equivalent liquid waveguide and evaluation of uncertainty," *Mathematical Biosciences and Engineering*, vol. 16, no. 6, p. 7911–7920, 2019. https://doi.org/10.3934/mbe.2019397.

[10] K. Pokovic, *Advanced electromagnetic probes for near-field evaluations*. Verlag nicht ermittelbar, 1999. https://doi.org/10.3929/ethz-a-003823823.

[11] V. Monebhurrun, "Effect of time-averaging of pulsed radio-frequency signals on specific absorption rate measurements," *IEEE Transactions on Electromagnetic Compatibility*, vol. 52, no. 1, pp. 49–55, 2010. https://doi.org/10.1109/TEMC.2009.2036370.

[12] A. K. Sharma and S. K. Dubey, "Real-world shelf-life study of tissue equivalent liquids for SAR evaluation," in *2022 URSI Regional Conference on Radio Science (USRI-RCRS)*, pp. 1–4, 2022. https://doi.org/10.23919/URSI-RCRS56822.2022.10118551.

[13] Z. Cendes, "The development of HFSS," in *2016 USNC-URSI Radio Science Meeting*, pp. 39–40, 2016. https://doi.org/10.1109/USNC-URSI.2016.7588501.

[14] B. Hakim, B. Beard, and C. Davis, "Precise dielectric property measurements and E-field probe calibration for Specific Absorption Rate measurements using a rectangular waveguide," *Measurement Science and Technology*, vol. 20, p. 045702, 02 2009. https://doi.org/10.1088/0957-0233/20/4/045702.

[15] M. Abdul-Al, A. S. I. Amar, I. Elfergani, R. Littlehales, N. Ojaroudi Parchin, Y. Al-Yasir, C. H. See, D. Zhou, Z. Zainal Abidin, M. Alibakhshikenari, C. Zebiri, F. Elmegri, M. Abusitta, A. Ullah, F. M. A. Abdussalam, J. Rodriguez, N. J. McEwan, J. M. Noras, R. Hodgetts, and R. A. Abd-Alhameed, "Wireless electromagnetic radiation assessment based on the Specific Absorption Rate (SAR): A review case study," *Electronics*, vol. 11, no. 4, 2022. https://doi.org/10.3390/electronics11040511.

[16] F. Seif, M. Omidi, M. R. Bayatiani, and M. Ghorbani, "Measurement and calculation of SAR due to 900 MHz electromagnetic waves," *Frontiers in Biomedical Technologies*, vol. 9, pp. 38–44, Dec. 2021. https://doi.org/10.18502/fbt.v9i1.8143.

Javier Samaniego Electronic Engineer from Ricardo Palma University. Researcher of the Direction of Research and Technological Development of INICTEL-UNI. Researcher in RENACYT, with several publications in congresses and indexed journals. He has participated in several international and national events on Non-Ionizing Radiation generated by mobile telephony. Likewise, he has experience in radio propagation projects, wireless communications oriented to access and broadband technologies.

Jorge Olivares Electronic Engineer, received his bachelor's degree in electronic engineering from the Universidad Nacional Pedro Ruíz Gallo, Perú, in 2019. In 2021 he completed his master's studies in software engineering at the Universidad Nacional Mayor de San Marcos. He is currently a Researcher at INICTEL-UNI. His research interests include wireless technologies (4G and 5G), IoT applications with artificial intelligence (AI), programming and development environments in cloud computing.

Rolando Adriano Engineer Adriano has an MSc with a mention in renewable energies and energy efficiency at the Universidad Nacional de Ingeniería. He is currently a doctoral candidate. Engineer Adriano has directed research projects as principal investigator and has developed different renewable energy prototypes. He is currently a research professor at the Faculty of Physical Sciences of the Universidad Nacional Mayor de San Marcos.

Brayan Pérez Physicist from the Universidad Nacional de Ingeniería. He is currently a master's candidate in AI and Big data at the Swiss School of Management. Participating researcher in health-related projects such as Analysis of thermal distribution in plasmonic photothermal therapies (2019), IOT Oximeter Prototype (2021), Dosimetric detector for commissioning in radiotherapy with LINAC (2023). He is currently in charge of analysis automation in the medical physics working group-UNI.

Saúl Inca Dr.-Ing., received his MSc. in Systems Technologies and Communication Networks and his Ph.D. degree in Telecommunications Engineering from the Universitat Politècnica de València (UPV) in 2014 and 2019. He is currently participating as a postdoctoral researcher in European Projects at the Institute of Telecommunications and Multimedia Applications. His main research areas are focused on radio channel modeling and the development of visualization platforms for 5G and B5G networks.

Marco Quispe Electronic Engineer from Universidad Nacional Mayor de San Marcos. RENACYT qualified researcher. He works in the Microwave and Optical Radiofrequency Coordination of INICTEL-UNI, supporting the formulation and execution of research projects and technological development and innovation (RDI) activities related to wireless communication systems in rural areas, Non-Ionizing Radiation and the implementation of 4G/5G mobile communication systems.